Author Manuscript

Author Manuscript

Author Manuscript

Author Manuscript

HHS Public Access

Author manuscript

Dev Biol. Author manuscript; available in PMC 2018 May 01.

Published in final edited form as:

Dev Biol. 2017 May 01; 425(1): 85–99. doi:10.1016/j.ydbio.2017.03.011.

Annexin A6 controls neuronal membrane dynamics throughout chick cranial sensory gangliogenesis

Ankita Shah, **Andrew T. Schiffmacher**, and **Lisa A. Taneyhill***

Department of Animal and Avian Sciences, University of Maryland, College Park, MD 20742, USA

Abstract

Cranial sensory ganglia are components of the peripheral nervous system that possess a significant somatosensory role and include neurons within the trigeminal and epibranchial nerve bundles. Although it is well established that these ganglia arise from interactions between neural crest and neurogenic placode cells, the molecular basis of ganglia assembly is still poorly understood. Members of the Annexin protein superfamily play key roles in sensory nervous system development throughout metazoans. Annexin A6 is expressed in chick trigeminal and epibranchial placode cell-derived neuroblasts and neurons, but its function in cranial ganglia formation has not been elucidated. To this end, we interrogated the role of Annexin A6 using gene perturbation studies in the chick embryo. Our data reveal that placode cell-derived neuroblasts with reduced Annexin A6 levels ingress and migrate normally to the ganglionic anlage, where neural crest cell corridors correctly form around them. Strikingly, while Annexin A6-depleted placode cell-derived neurons still express mature neuronal markers, they fail to form two long processes, which are considered morphological features of mature neurons, and no longer innervate their designated targets due to the absence of this bipolar morphology. Moreover, overexpression of Annexin A6 causes some placode cell-derived neurons to form extra protrusions alongside these bipolar processes. These data demonstrate that the molecular program associated with neuronal maturation is distinct from that orchestrating changes in neuronal morphology, and, importantly, reveal Annexin A6 to be a key membrane scaffolding protein during sensory neuron membrane biogenesis. Collectively, our results provide novel insight into mechanisms underscoring morphological changes within placode cell-derived neurons that are essential for cranial gangliogenesis.

Keywords

cranial ganglia; placode cells; neural crest cells; Annexin A6; membrane dynamics; neurons

*Address for manuscript correspondence: ltaney@umd.edu, Tel: 301 405 0597, Fax: 301 405 7980.

Publisher's Disclaimer: This is a PDF file of an unedited manuscript that has been accepted for publication. As a service to our customers we are providing this early version of the manuscript. The manuscript will undergo copyediting, typesetting, and review of the resulting proof before it is published in its final citable form. Please note that during the production process errors may be discovered which could affect the content, and all legal disclaimers that apply to the journal pertain.

Author Manuscript Author Manuscript Author Manuscript Author Manuscript

INTRODUCTION

The cranial ganglia of the peripheral nervous system are important for integrating and relaying sensory information. These ganglia arise from the intermixing and coalescence of two different embryonic populations, neural crest and neurogenic placode cells (Hamburger, 1961) (Park and Saint-Jeannet, 2010) (Saint-Jeannet and Moody, 2014) (Steventon et al., 2014). During development, placode cells ingress from the overlying ectoderm and enter the mesenchyme where they proliferate and differentiate into multipolar neuroblasts (Steventon et al., 2014) (Smith et al., 2015). As the neuroblasts mature into neurons, they interact with migratory neural crest cells that originate from the dorsal neural tube or folds to create the ganglia (Hamburger, 1961) (Steventon et al., 2014) (Shiau et al., 2008). Neural crest cells, however, do not differentiate into neurons until later (D'Amico-Martel and Noden, 1980) (Steventon et al., 2014) such that the initial population of ganglion neurons is derived solely from placode cells.

As the cranial ganglia assemble, neural crest cells are thought to provide a scaffold for placode cell-derived neurons, which then mediate neural crest condensation (Shiau et al., 2008). Furthermore, neural crest cells form corridors that surround these neurons, providing them with the proper local environment to promote migration and later ganglia formation (Freter et al., 2013). Multipolar neuroblasts entering the ganglionic anlage eventually undergo "neuronal maturation" in which they adopt a bipolar morphology and exit the cell cycle. Importantly, this maturation process in the chick epibranchial system has been proposed to be governed by distinct stages of gene expression, and cell morphologies, defining the sequential progression from a placode cell to a mature neuron (Smith et al., 2015). The pathways that control the differentiation and maturation of placode cells into sensory neurons, as well as the mechanisms underlying cell morphology changes and subsequent neural crest-placode cell interactions during ganglia assembly, however, remain elusive.

One of the driving forces underlying cell migration and intercellular interactions is the reorganization of cell membranes and remodeling of the cytoskeleton, processes facilitated by Annexin proteins in multiple systems. The Annexin protein superfamily is highly conserved during nervous system development across metazoans. Gastropod snails express various Annexin-like proteins in their neurons (Kerschbaum et al., 1997), while Annexin A6 is present in dorsal root ganglia neurons and motor neuron precursors within developing mouse and rat spinal cords (Naciff et al., 1996). Moreover, cultured mouse olfactory and hippocampal neurons gradually concentrate Annexin A6 into maturing axons, which show enhanced branching upon Annexin A6 overexpression (Yamatani et al., 2010). In the chick, our prior work revealed that Annexin A6 modulates early cranial neural crest cell migration (Wu and Taneyhill, 2012). Intriguingly, later in chick development, Annexin A6 is expressed in trigeminal and epibranchial placode cell-derived neuroblasts and is maintained in these neurons throughout ganglia assembly (Shah and Taneyhill, 2015). The function of Annexin A6 during cranial gangliogenesis, however, has not been elucidated.

To this end, we interrogated the role of Annexin A6 using gene perturbation studies in the chick embryo. Our results show that placode cell-derived neuroblasts depleted for Annexin

Author Manuscript Author Manuscript Author Manuscript Author Manuscript

A6 ingress and migrate normally to the ganglionic anlage, where they correctly interact with neural crest cells. Interestingly, while Annexin A6-depleted neurons still express mature neuronal markers, they form very short, and in some instances, no processes, which are thought to be features associated with mature neurons, and thus do not adopt a bipolar cell morphology. As such, these placode cell-derived neurons no longer innervate their targets. Furthermore, Annexin A6 overexpression causes some of these neurons to generate additional protrusions from their bipolar processes. These findings indicate that the molecular programs controlling gene expression and neuronal morphology changes are distinct, and reveal Annexin A6 to be a critical membrane scaffold for the dynamic remodeling of sensory neuron membranes during ganglia formation. Taken together, our data shed new light on how placode cell-derived neurons adopt a bipolar morphology that is vital for proper cranial ganglia assembly.

MATERIALS AND METHODS

Chick embryos

Fertilized chicken eggs (Gallus gallus) were obtained from Centurion Poultry (GA) and incubated at 37°C in humidified incubators. Embryos were staged by the Hamburger-Hamilton (HH) staging method (Hamburger and Hamilton, 1992).

Annexin A6 MO and expression constructs

A 3′ lissamine-tagged antisense Annexin A6 morpholino (MO) (5′-GTAAACCTTTCCTTTGGGTGCCATG-3′), along with a 5 base pair (bp) mismatch (shown in lower case) lissamine-tagged antisense Annexin A6 control MO (5′-GTAtAgCTTTgCTTTcGcTGCCATG-3′), were designed to target *Annexin A6* according to the manufacturer's criteria (GeneTools, LLC). These MOs were used at a concentration of 500 μM to prevent translation of *Annexin A6* mRNA (in the case of the antisense Annexin A6 MO). The full-length cDNA for chick *Annexin A6* was PCR-amplified from HH14–16-dissected chick trigeminal ganglia and cloned into the pCIG expression construct. Primers were chemically synthesized and PAGE-purified (Integrated DNA Technologies, Coralville, Iowa, USA). All clones were sequenced to ensure sequence accuracy. The control (pCIG) or pCIG-Annexin A6 expression construct was introduced into the embryo at a concentration of 2.5 μg/μl.

5′ and 3′ RACE

Rapid amplification of cDNA ends (RACE) was carried out using the SMARTer RACE 5′/3′ Kit according to the manufacturer's instructions (Takara Bio USA, Mountain View, CA, USA). All RACE reactions and controls were performed using both total cellular RNA collected from HH15–17 trigeminal ganglia and enriched poly(A) mRNA from HH15–17 heads (NucleoTrap® mRNA, Takara Bio USA). Two gene-specific primers (5′-GATTACGCCAAGCTT-CCTGGTTGGTGCGGGAGGCGAGGATCTC-3′ and 5′-GATTACGCCAAGCTT-CATCCGATAGGCCACCTGCGCTGCCTCC-3′) were designed with 5′ fusion overhangs (underlined) and used to amplify 5′ ends from 5′ RACE-ready cDNAs. One gene-specific primer was used to amplify the 3′ end (5′-GATTACGCCAAGCTT-GGCAGCGCAGGTGGCCTATCGGATGTGG-3′; Integrated

Author Manuscript Author Manuscript Author Manuscript Author Manuscript

DNA Technologies, Coralville, Iowa, USA). Twenty-four 5′ RACE clones and ten 3′ RACE clones were sequenced to identify consensus transcriptional variants (Genewiz, South Plainfield, NJ, USA).

In ovo ectodermal electroporation technique

MOs or expression constructs were introduced into the placodal ectoderm at HH8–11 (prior to ingression) in order to target both placode cells and their eventual neuronal derivatives in the ganglionic anlage. Electroporations were carried out as described in (Shiau et al., 2008). Briefly, after filling the topical midbrain ectoderm with the MO or expression construct, platinum electrodes were placed vertically across the chick embryo to deliver three current pulses of 9 V over 50 milliseconds at 200 millisecond intervals. Eggs were resealed with tape and parafilm and reincubated for approximately 18–24 hours to reach HH13–14, approximately 28–36 hours to reach HH15–16, or approximately 40–52 hours to reach HH17–19, prior to harvesting for further experimentation.

Immunoblotting

Protein extraction and immunoblotting was performed as described in (Schiffmacher et al., 2014). Neural tubes electroporated with either the Annexin A6 or control MO were excised 6–8 hours post-electroporation, pooled, pelleted, flash-frozen in liquid nitrogen, and stored at −80 C until needed for immunoblot analysis. Pellets were thawed on ice and lysed in lysis buffer (50 mM Tris pH 8.0, 150 mM NaCl, 1% IGEPAL CA-630) supplemented with cOmplete protease inhibitor cocktail (Roche, Basel, Switzerland) and 1 mM PMSF for 30 minutes at 4 C with periodic mixing. Soluble fractions were collected following centrifugation at max g for 15 minutes at 4 C, and protein concentration was quantified by Bradford assay (Thermo Fisher Scientific, Rockford, IL, USA). Equivalent amounts of protein per sample were boiled at 100 °C for 5 minutes in 4X reducing Laemmli sample buffer and then centrifuged at max g for 5 minutes at room temperature. Supernatants were processed by SDS-PAGE (Bio-Rad, Hercules, CA) and then transferred to 0.45 μm BioTrace PVDF membrane (Pall, Port Washington, NY). Primary antibodies used for immunoblotting were Annexin A6 (1:2000, PAB18085, ABNOVA, Taipei City, Taiwan) and GAPDH (1:2500, MA515738, Thermo Fisher Scientific). Immunoblot images for figures were gamma-modified and processed using Photoshop 9.0 (Adobe Systems, San Jose, CA, USA). Immunoblot band volumes (intensities) were calculated from unmodified immunoblot images using Image Lab software (Bio-Rad, Hercules, CA, USA), and relative protein levels were calculated by normalizing Annexin A6 band volumes to GAPDH band volumes. Differences in the amount of Annexin A6 were assessed by comparing normalized ratios between control MO- and Annexin A6 MO-treated samples, with the control MO-treated sample set at one.

Immunohistochemistry and TUNEL assay

Immunohistochemical detection of Tubb3 (Abcam, 1:500), HNK-1 (Developmental Studies Hybridoma Bank, 1:100), HuC/D (Life Technologies, 1:200), Neurofilament-M (Life Technologies, 1:200), phospho-histone H3 (Millipore, 1:200), and GFP (Invitrogen, 1:250) was performed on 10 μm transverse sections following 4% PFA fixation and gelatin embedding. Annexin A6 (Abnova; 1:100) immunostaining was carried out on transverse

Author Manuscript Author Manuscript Author Manuscript Author Manuscript

sections as described in previous studies (Shah and Taneyhill, 2015). After de-gelatinizing the sections on the slides, the sections were blocked for 1–2 hours in 1X phosphate-buffered saline + 0.1% TritonX-100 (PBSTX) + 10% sheep serum. All primary and secondary antibodies were diluted in PBSTX + 5% sheep serum. Appropriate fluorescently-conjugated secondary antibodies (Alexa Fluor 488, 594, 647; Life Technologies) were used at a concentration of 1:500. Sections were mounted using Fluoromount G that contains 4′,6-diamidino-2-phenylindole (DAPI). The TUNEL assay (Roche, TMR red and fluorescein) was performed on de-gelatinized sections to detect apoptotic cells as in (Wu et al., 2014). For all experiments, images were acquired using a Zeiss LSM800 confocal microscope at 40X and 63X magnifications, and data processing was conducted using Adobe Photoshop 9.0.

Confocal Imaging

For all experiments, images of at least five serial transverse sections through a minimum of eight embryos (unless indicated otherwise) were acquired with the LSM Zeiss 800 confocal microscope at 40× and 63× magnifications. Where possible, the laser power, gain, and offset were kept consistent for the different channels throughout experiments. The pinhole was always set to one airy unit. The Z-section optical images were acquired between 0.25 and 0.4 μm per optical section and reconstituted in 3D composites using the Zen software (Zeiss Zen 2.0).

Measurement of neuronal processes

To measure the length of neuronal processes upon Annexin A6 depletion, confocal imaging of the trigeminal ganglionic anlage containing both control MO- and Annexin A6 MO-positive cells was performed at 63X magnification. Measurements of each of the two morphological types of neurons (control MO: bipolar; Annexin A6 MO: short projections) were performed using the Zeiss Zen 2.0 software from Z-stacks generated from at least five serial sections through a minimum of five each control MO- and Annexin A6 MO-electroporated embryos. Results are reported as means +/− standard deviation and standard error of the mean, with statistical significance of data established using an unpaired student's *t* test (Schiffmacher et al., 2014) (Wu et al., 2014).

RESULTS

Two *Annexin A6* transcript variants exist in the chick head

Computational searches for chick *Annexin A6* mRNA sequences in ENSEMBL and NCBI databases yielded multiple predicted and referenced sequences with highly variable 5′ UTRs, which precluded the design of a universal *Annexin A6* morpholino (MO). To first verify the sequences in these databases, we performed 5′ and 3′ RACE. From all 5′ RACE reactions generated from either HH14–17 trigeminal ganglia total cellular RNA or HH14–17 head poly (A) mRNA and 2 gene-specific primers, we identified two distinct noncoding 5′ UTRs that compose alternate first exons (Fig. 1A). Exon 1A is identical to a previously validated *Annexin A6* sequence (NCBI Accession NM_204730.1), although 12% of these clones possessed an additional 14–21 nucleotides at the 5′ end. The 3′ half of the exon 1B sequence is conserved with predicted variant sequences (NCBI Accessions

Author Manuscript Author Manuscript Author Manuscript Author Manuscript

XM_015293732.1 and XM_015293733.1) but is truncated at the 5′ end. Both exons 1A and 1B share a common splice acceptor site to the conserved exon 2, which contains the ATG start codon. Sequences for 3′ RACE yielded a single 3′ UTR identical to NCBI Accession NM_204730.1.

Because both variants possess a common ATG start codon and upstream sequence found in exon 2, we designed a translation-blocking MO that would target both transcript variants. This MO is specific to *Annexin A6*, as demonstrated by a search of the chick genome, which revealed a lack of targeting of the MO to all documented chick *Annexin* transcripts (Fig. 1B). In further support of this, we explored the chick *in situ* hybridization database (GEISHA) to identify other possible *Annexins* that the Annexin A6 MO could potentially target. Although expressed in the chick, we found that *Annexins A1*, *A2*, *A4-like*, *A5*, and *A11* are not observed in trigeminal and epibranchial placode cells. The expression for the remaining three in this database (*Annexins A7*, *A8*, and *A10*) have not been examined at the older embryo stages we have used in our studies; however, these *Annexins* are not at all expressed in placodal precursor cells (HH8: no expression for *Annexins A7* and *A8*; HH10: no expression for *Annexins A7*, *A8*, and *A10*). Furthermore, the primary Annexins that function in the rat and mouse during nervous system development are Annexin A2 (Ning et al., 2012) (Avenali et al., 2014) (Yamanaka et al., 2016) and A7 (Lessner et al., 2010) (Rick et al., 2005), which, as discussed above, are not expressed in the appropriate spatio-temporal pattern to play a role in the formation of the chick cranial sensory ganglia. Taken together, these data indicate that our translation-blocking MO to *Annexin A6* targets its two transcript variants.

To examine the efficacy of the Annexin A6 MO in depleting Annexin A6 protein, we electroporated a 5 bp mismatch Annexin A6 control MO, or the Annexin A6 MO, and collected electroporated tissue after 6–8 hours in order to examine degree of Annexin A6 knockdown by immunoblotting (Fig. 1C), as in (Wu and Taneyhill, 2012). Immunoblotting for Annexin A6 reveals a 34% reduction in Annexin A6 protein, consistent with what we have observed in our prior work with a similar translation-blocking MO targeting *Annexin A6* (Wu and Taneyhill, 2012). This MO was then used for the studies described below to address the function of Annexin A6 during gangliogenesis.

Annexin A6 depletion from trigeminal placode cells does not affect their ingression, differentiation, or position within the ganglionic anlage

Our previous studies demonstrated that Annexin A6 is expressed predominantly on the membrane of placodal sensory precursors in the ectoderm and their neuronal derivatives that have ingressed into the mesenchyme (Shah and Taneyhill, 2015). To determine the function of Annexin A6 within cranial sensory neurons, we used an ectodermal electroporation method described previously (Shiau et al., 2008) to introduce the control or Annexin A6 MO into the precursor sensory ectoderm at Hamburger-Hamilton (HH) 10. Embryos were then reincubated to assess effects on the ingression of trigeminal placode cell-derived neurons as well as their differentiation (Fig. 2). Knockdown of Annexin A6 in trigeminal placode cells reveals that their neuronal derivatives ingress normally into the mesenchyme from the trigeminal ectoderm (Fig. 2E, H′, arrows), and that these neurons get correctly positioned in

Author Manuscript Author Manuscript Author Manuscript Author Manuscript

the ganglionic anlage (Fig. 2G), as noted for control MO-treated embryos (Fig. 2A, C, arrows). Importantly, Annexin A6 MO-containing neurons have reduced signal for Annexin A6 protein (Fig. 2F, H′, arrowheads, n = 11 ganglia) compared to neurons in the control MO-containing embryo (Fig. 2B, D′, arrowheads, n = 9 ganglia), further validating the specificities of the Annexin A6 MO and antibody. We also observe comparable results for epibranchial neurons depleted for Annexin A6 since they possess a similar pattern of Annexin A6 expression and subsequent neurogenesis (see (Shah and Taneyhill, 2015) (Smith et al., 2015); data not shown). Collectively, our results indicate that depletion of Annexin A6 from trigeminal or epibranchial neuronal precursors does not adversely affect trigeminal or epibranchial neuron ingression, differentiation, or position.

Knockdown of Annexin A6 impacts projection outgrowth from cranial sensory neurons

As neuronal morphology is an important component of placodal neurogenesis (Smith et al., 2015), we next examined the morphology of Annexin A6-depleted sensory neurons within the ganglionic anlage. Using the above Annexin A6 MO knockdown approach, we electroporated placodal ectoderm at HH9-10 and collected embryos at HH16-17 when trigeminal and epibranchial (here the geniculate) bipolar neurons are forming nerves within the ganglia. To evaluate neuronal and overall ganglion morphology, we performed immunohistochemistry for Tubb3 (Moody et al., 1989; Shiau et al., 2008; Wu et al., 2014), the class III β-tubulin in neurons either in their last stage of, or upon their exit, from the cell cycle (Moody et al., 1989), and examined tissue sections of forming trigeminal and geniculate ganglia (Figs. 3 and 4), and the trigeminal ganglion in lateral, whole-mount views (Fig. 5), in the presence or absence of Annexin A6.

Trigeminal (Fig. 3A-C') and geniculate (Fig. 3G-I') neurons at HH16 containing control MO exhibit a bipolar morphology with neuronal processes marked by Tubb3 (trigeminal, Fig. 3B-C', n=9 ganglia; geniculate, Fig. 3H-I', n=9 ganglia; Smith et al., 2015). Trigeminal (Fig. 3D-F') and geniculate (Fig. 3J-L') neurons containing Annexin A6 MO and exhibiting a reduction in Annexin A6, however, possess a few short or even no projections, and many in fact appear round (trigeminal, Fig. 3E-F', n=10 ganglia; geniculate, Fig. 3K-L', n=10 ganglia). Overall, more than 95.5% of Annexin A6-depleted neurons possess short or no projections (n=7 ganglia, 779 neurons counted; 744 neurons ± 7.56 (standard deviation) or ± 0.277 (standard error of the mean) exhibit a phenotype; see Table S1), while all control MO-containing neurons have a bipolar morphology (n=7 ganglia, 836 neurons counted). Furthermore, trigeminal (Fig. 3C', arrows) and geniculate (Fig. 3I', arrows) neurons containing control MO possess neuronal processes that form nerve bundles with the neighboring neurons. Conversely, those neurons containing Annexin A6 MO (trigeminal, Fig. 3F', arrows; geniculate, Fig. 3L', arrows) are positioned correctly within the ganglionic anlage but have shorter, or even lack, neuronal processes arising from their cell bodies, and therefore are likely to not form subsequent nerve bundles.

We next quantified the length of neuronal processes of Annexin A6 MO- and control MO-containing trigeminal neurons using Tubb3 as a marker (Fig. 4). The average process length of control MO-containing trigeminal neurons (Fig. 4A, A', arrows) is almost three times longer (25.1 μm ± 9.27 μm (standard deviation) or ± 1.49 μm (standard error of the mean);

Author Manuscript Author Manuscript Author Manuscript Author Manuscript

n=5 ganglia, 39 neurons measured) than the Annexin A6 MO-containing trigeminal neurons (9.49 μm ± 3.12 μm (standard deviation) or ± 0.551 μm (standard error of the mean); n=5 ganglia, 32 neurons measured) (Fig. 4B, B', arrowheads, Table S2), and this result is highly statistically significant (p=1.71E-13). Furthermore, many of the Annexin A6 MO-containing neurons possess truncated processes emanating from their cell bodies, or none at all (Fig. 4C, C', caret).

Given the drastic morphology change observed in sensory neurons with reduced Annexin A6 levels, we performed confocal imaging of whole embryo heads electroporated with the control or Annexin A6 MO to examine gross trigeminal ganglion morphology. Embryos treated with the control MO exhibit a condensed, compact trigeminal ganglion, with forming nerve bundles (Fig. 5A–C, arrows, n = 5 ganglia in 4 embryos). Conversely, we observe a disruption in overall trigeminal ganglion morphology in Annexin A6-depleted embryos (Fig. 5D–F, arrows, n = 11 ganglia in 6 embryos; stage-matched with control MO-treated embryos). Specifically, the neurons appear disorganized and dispersed, and the overall ganglion is less condensed due to the absence of nerve bundles (attributed to the short to no processes now present upon Annexin A6 depletion), when compared to control MO-treated embryos (100% of Annexin A6 MO-containing ganglia show an altered morphology compared to 0% of control MO-containing ganglia). Taken together, these data suggest that Annexin A6 may have a role in the outgrowth of neuronal processes during cranial sensory neurogenesis.

Annexin A6-depleted sensory neurons fail to innervate their designated targets later in development

Trigeminal placode cells differentiate into sensory neurons of cranial nerve V and innervate the sensory apparati in the muscles of the eye region, upper and lower jaw, as well as the tongue (Gillig and Sanders, 2010). Based on our results above revealing truncated to absent outgrowth of processes in neurons with decreased Annexin A6, we next examined older embryos when these neurons are innervating their targets. We electroporated placodal ectoderm at HH9–10 and collected embryos at HH19–20, when the maxillary and mandibular branches of the trigeminal bipolar neurons have made their way ventrally to innervate the pharyngeal arches. To evaluate the formation of processes in these neurons upon Annexin A6 depletion, we performed Tubb3 immunohistochemistry (Fig. 6), which, at this stage of development, will only label placodal neurons since neural crest cells do not differentiate until HH22–24 (D'Amico-Martel and Noden, 1980). Control MO-containing trigeminal neurons (Fig. 6A–C′) with neuronal processes (Fig. 6B, C) form nerves that innervate the pharyngeal arches (Fig. 6C′, arrows, n = 7 ganglia, 91 neurons counted +/− 1.49 (standard deviation) or +/− 0.156 (standard error of the mean); all show this phenotype). Although Annexin A6 MO-containing trigeminal neurons (Fig. 6D–F′) travel to the pharyngeal arches and maintain their proper identity, as seen by Tubb3 in their cell bodies (Fig. 6E–F′), these neurons still possess few short to no processes and thus will not innervate the sensory apparati in the muscles (Fig. 6F′, arrows, n = 8 ganglia). Quantification reveals that 94.2% of Annexin A6-depleted neurons that reach the pharyngeal arches do not possess a bipolar morphology (Table S3, n = 5 ganglia, 103 neurons counted; 97 neurons +/− 1.64 (standard deviation) or +/− 0.166 (standard error of the mean) exhibit

Author Manuscript Author Manuscript Author Manuscript Author Manuscript

this phenotype). Altogether, these results further corroborate that Annexin A6 functions during the formation of processes within these cranial sensory neurons.

Sensory neurons with reduced Annexin A6 levels express neuronal maturation markers despite having an altered morphology

An important feature exhibited by a sensory neuron during its maturation is the change from a multipolar to bipolar morphology. This morphological transition is correlated with the onset of expression of specific markers and is referred to generally as “neuronal maturation” (Smith et al., 2015). As Annexin A6-depleted neurons do not adopt a bipolar morphology, we wondered whether these neurons in fact mature from a molecular standpoint. To this end, we examined these neurons for expression of HuC/D (Fig. 7) and Neurofilament-M (NFM) (Fig. 8), additional markers of mature neurons. HuC/D is an RNA binding protein that is only expressed in mature, post-mitotic neurons (Blentic et al., 2011; Smith et al., 2015), whereas NFM is a component of intermediate filaments comprising the axoskeleton of mature neurons that mediates radial projection growth and intracellular transport to axons (Perrot et al., 2008; Smith et al., 2015). We electroporated placodal ectoderm at HH9-10 and collected embryos at HH16-17, when the trigeminal neurons should be morphologically bipolar. Trigeminal neurons containing control MO (Fig. 7A-D’) marked by Tubb3 (Fig. 7C, D) express HuC/D (Fig. 7B, D, D’, arrows, n=7 ganglia). Interestingly, trigeminal neurons depleted for Annexin A6 (Fig. 7E-H’) also express HuC/D (Fig. 7F, H, H’, arrows), even when these neurons possess few short to no processes as seen by Tubb3 in their cell bodies (Fig. 7G, H, n=8 ganglia). Likewise, trigeminal neurons containing either control MO (Fig. 8A-D’) or Annexin A6 MO (Fig. 8E-H’) express NFM (Fig. 8B, D, D’, arrows, n=5 ganglia; Fig. 8F, H, H’, arrows, n=7 ganglia; respectively). Thus, our data indicate that Annexin A6 knockdown has no effect on the expression of neuronal maturation markers even though these neurons possess shorter or no processes, revealing that the expression of these mature neuronal markers is distinct from the morphology change that accompanies “neuronal maturation,” as currently defined for petrosal placode cell-derived neurons (Smith et al., 2015).

Annexin A6-depleted sensory neurons have no adverse effects on the surrounding neural crest cells during ganglia assembly

During cranial ganglia assembly, neural crest cells provide a favorable local environment for migrating sensory neurons by forming a pocket or corridor. This corridor surrounds and encloses the sensory neurons while they send out processes and assemble the nerves (Freter et al., 2013). Importantly, interactions between neural crest cells and sensory neurons are required for proper corridor formation and subsequent ganglia assembly (Freter et al., 2013) (Shiau et al., 2008). To evaluate potential effects on cranial neural crest cells surrounding Annexin A6-depleted sensory neurons, we performed Annexin A6 knockdown in the precursor placode cell population as described previously and examined migratory neural crest cells through immunohistochemistry for HNK-1 (Fig. 9). Embryos electroporated with the control MO within trigeminal (Fig. 9A–D′) and geniculate (Fig. 9I–L′) neurons at HH16 exhibit normal neural crest cell corridors surrounding these neurons (trigeminal, Fig. 9B, D, D′, arrows, n = 10 ganglia; geniculate, Fig. 9J, L, L′, arrows, n = 7 ganglia), with the core bipolar sensory neurons marked by Tubb3 (trigeminal, Fig. 9C–D′; geniculate, Fig. 9K–L′).

Author Manuscript Author Manuscript Author Manuscript Author Manuscript

Interestingly, embryos in which trigeminal and geniculate neurons are depleted for Annexin A6 (Fig. 9E–H′ and Fig. 9M–P′, respectively) also form intact neural crest cell corridors (trigeminal, Fig. 9F, H, H′, arrows, n = 11 ganglia; geniculate, Fig. 9N, P, P′, arrows, n = 8 ganglia), despite these neurons having few short to no processes (trigeminal, Fig. 9G–H′; geniculate, Fig. 9O–P′). Collectively, our data reveal that a reduction in Annexin A6, and subsequent loss of neuronal processes, has no impact on the ability of the surrounding neural crest cells to form intact corridors around these sensory neurons.

Trigeminal neurons overexpressing Annexin A6 are positioned correctly within the ganglionic anlage but in some instances possess alterations in membrane morphology

Since Annexin A6-depleted trigeminal and epibranchial neurons showed few to no projections using Tubb3, we next examined effects of Annexin A6 overexpression in these neurons. Using the above described electroporation approach, we electroporated placodal ectoderm at HH9-10 and collected embryos at HH16-17 when the trigeminal bipolar neurons have begun to form nerves within the ganglia. To evaluate neuronal morphology, we performed immunohistochemistry for Tubb3. Trigeminal (Fig. 10A-D') neurons at HH16 electroporated with the control vector (Fig. 10A) exhibit a bipolar morphology with neuronal processes marked by Tubb3 (Fig. 10B, D, D'), which colocalizes with endogenous Annexin A6 (Fig. 10C-D', arrows, n=15 ganglia). Trigeminal (Fig. 10E-H') neurons overexpressing Annexin A6 (Fig. 10E) also possess bipolar neuronal processes, are positioned correctly within the ganglionic anlage, and express Tubb3 (Fig. 10F, H, H', arrows, n=15 ganglia), and are therefore likely to later form nerves and innervate their designated targets. Intriguingly, some of these electroporated neurons possess extra protrusions emanating from their membranes that are Annexin A6-positive but not always immunoreactive for Tubb3 (Fig. 10H, H', arrowheads; see also Fig. 11, with arrows showing these neurons at a higher magnification, and Table S4). Although this phenotype is observed, on average, in 35.2% of the electroporated sensory neurons analyzed (138 neurons with pCIGAnnexin A6 having multiple protrusions ± 3.05 (standard deviation) or ± 0.259 (standard error of the mean)), all of the examined ganglia (n=7 ganglia, 392 neurons counted) possess cells with these additional protrusions upon Annexin A6 overexpression. None of the analyzed neurons exhibit this phenotype, however, in control embryos (n=7 ganglia, 337 neurons counted; 0 neurons with pCIG having multiple protrusions). Given their normal positioning in the ganglionic anlage and the fact that only a minority of the sensory neurons overexpressing Annexin A6 possesses extra protrusions, we were unable to detect any changes in overall ganglion organization and morphology in lateral views of whole embryo heads after Annexin A6 overexpression (data not shown). Taken together with our knockdown studies, these results implicate Annexin A6 in controlling membrane outgrowth in placode cell-derived neurons, and overall sensory neuron morphology, during cranial gangliogenesis.

Annexin A6 perturbation does not impact cell death and cell proliferation in the trigeminal neurons during ganglia formation

With our Annexin A6 knockdown and overexpression results showing changes in cell morphology, including truncated to absent or additional neuronal processes, respectively, in the sensory neurons, and subsequent loss of target innervation after Annexin A6 depletion,

Author Manuscript Author Manuscript Author Manuscript Author Manuscript

we wanted to rule out any potential non-specific effects that might be caused by introduction of the Annexin A6 MO or expression construct. As such, we performed cell proliferation (phospho-histone H3 immunohistochemistry) and cell death (TUNEL) assays (Wu et al., 2014) (Fig. S1). To this end, we electroporated trigeminal placodes at HH9–10 and collected embryos at HH15–16. We observe no change in the amount of cell death after electroporation of the control MO (Fig. S1A, arrows; n = 5 ganglia, 716 electroporated neurons counted; 6 neurons double-positive for control MO and TUNEL +/− 0.407 (standard deviation) or +/− 0.166 (standard error of the mean); 0.838% of control MO-containing neurons are TUNEL-positive) or Annexin A6 MO (Fig. S1B, arrows; n = 5 ganglia, 894 electroporated neurons counted; 10 neurons double-positive for Annexin A6 MO and TUNEL +/− 0.492 (standard deviation) or +/− 0.156 (standard error of the mean); 1.12% of Annexin A6 MO-containing neurons are TUNEL-positive, $p = 0.158$; see Table S5). Furthermore, electroporation of both control vector (Fig. S1C, arrows; n = 5 ganglia, 514 electroporated neurons counted; 1 neuron is double-positive for pCIG and TUNEL +/− 0.196 (standard deviation or standard error of the mean); 0.195% of pCIG-containing neurons are TUNEL-positive) and the Annexin A6 expression construct (pCIG-Annexin A6, Fig. S1D, arrows; n = 5 ganglia, 473 electroporated neurons counted) also show a similar amount of cell death ($p = 0.313$; none of the pCIG-Annexin A6-containing neurons is TUNEL-positive; see Table S5). Likewise, we note no difference in cell proliferation in control (Fig. S1E, arrows; n = 5 ganglia, 636 neurons counted; 5 neurons are double-positive for control MO and phospho-histone H3 +/− 0.396 (standard deviation) or +/− 0.177 (standard error of the mean); 0.786% of control MO-containing neurons are phospho-histone H3-positive) or Annexin A6-depleted embryos (Fig. S1F, arrows; n = 5 ganglia, 724 neurons counted; 7 neurons are double-positive for Annexin A6 MO and phospho-histone H3 +/− 0.447 (standard deviation) or +/− 0.169 (standard error of the mean); 0.967% of Annexin A6 MO-containing neurons are phospho-histone H3-positive, $p = 0.552$; see Table S5). Comparable amounts of cell proliferation are also observed in neurons containing pCIG (Fig. S1G, arrows; n = 5 ganglia, 363 electroporated neurons counted; 1 neuron is double-positive for pCIG and phospho-histone H3 +/− 0.196 (standard deviation or standard error of the mean); 0.275% of pCIG-containing neurons are phospho-histone H3-positive) and pCIG-Annexin A6 (Fig. S1H, arrows; n = 5 ganglia, 546 electroporated neurons counted, $p = 0.322$; none of the pCIG-Annexin A6-containing neurons is phospho-histone H3-positive; see Table S5). Altogether, these results indicate that the morphology change observed in these mature sensory neurons upon knockdown or overexpression of Annexin A6 is likely due to the inherent requirement of Annexin A6 for membrane outgrowth during placodal neurogenesis and ganglia assembly as opposed to any changes in overall cellular activities such as cell death or proliferation.

DISCUSSION

Developing sensory neuroblasts require the spatio-temporal expression of different genes, along with dynamic changes in cell shape, in order to form mature, functional neurons and assemble the cranial ganglia. How these changes in gene expression relate to essential morphological alterations in these neurons, however, is still not known. Our previous studies revealed that Annexin A6 is expressed in placode cell-derived neuroblasts and neurons

Author Manuscript Author Manuscript Author Manuscript Author Manuscript

during chick gangliogenesis (Shah and Taneyhill, 2015). Herein, we demonstrate that the chick embryo head contains two *Annexin A6* transcripts with a common translational start site, allowing both variants to be targeted by the same translation-blocking MO to address Annexin A6 function. With this 34% reduction in Annexin A6 protein, cranial sensory neurons still ingressed into the mesenchyme, differentiated, and were positioned correctly in the ganglionic anlage. Additionally, we observe that cranial neural crest cells continue to surround Annexin A6-depleted sensory trigeminal and epibranchial neurons, forming corridors that are essential for correct ganglion assembly. Notably, our results highlight that precise Annexin A6 expression in developing placode cell-derived sensory neurons is critical for controlling cell membrane dynamics and overall morphology of these neurons, permitting the formation of neuronal processes and eventual sensory gangliogenesis. Given that we only achieved a partial knockdown of Annexin A6, it is possible that Annexin A6 may play an even larger role in placodal gangliogenesis than is presented herein.

Molecular programs governing sensory neuronal maturation and morphology changes are distinct

Prior work has shown that a sensory neuron is termed “mature” both when it expresses particular neuronal markers and exhibits a bipolar morphology, as described for petrosal neurons (Smith et al., 2015). Our data herein reveal that trigeminal and geniculate sensory neurons depleted for Annexin A6 undergo major membrane and subsequent cell shape changes. These neurons do not attain a “mature” bipolar morphology consisting of two long processes emanating from their cell bodies, as visualized through Tubb3, but still mature, from a molecular standpoint, because they express the neuronal markers Tubb3, HuC/D, and NFM. This absence of a bipolar morphology, in the presence of mature neuronal markers, indicates that these two events during neurogenesis are distinct from a molecular standpoint. Therefore, the current definition of “neuronal maturation” may require revisiting given this disconnect between neuronal gene expression and switch in cell morphology. These results suggest that sensory neurogenesis is highly complex and involves independent, yet required, molecular programs that control neuronal gene expression and orchestrate changes in cell shape.

Annexin A6 perturbations lead to dynamic morphological changes in the cell membranes of trigeminal and epibranchial neurons

Annexin A6-depleted trigeminal and epibranchial (here, geniculate) neurons possess few tiny processes that are significantly shorter than their normal counterparts. These neurons progressively mature but continue to have short or even no processes, as observed by class III β-tubulin distribution. Over the course of sensory gangliogenesis, the first of the trigeminal neurons derived from the maxillary-mandibular branch to arrive at the pharyngeal arches are termed pioneer neurons (Moody et al., 1989). Remarkably, we note that Annexin A6-depleted pioneer trigeminal neurons travel ventrally to the pharyngeal arches, albeit possessing no bipolar processes. These observations further validate our results and indicate that Annexin A6 impacts the formation of neuronal processes, and eventual nerves, with its loss negatively affecting innervation of target tissues. We believe comparable results for epibranchial neurons that form nerve fibers for cranial nerves VII, IX, and X would be noted

Author Manuscript Author Manuscript Author Manuscript Author Manuscript

since they follow similar patterns of Annexin A6 expression and neurogenesis (Shah and Taneyhill, 2015) (Smith et al., 2015).

Trigeminal neurons overexpressing Annexin A6 possess long bipolar neuronal processes with no adverse effects on Tubb3 distribution or expression. When observed later in development, these pioneer trigeminal neurons still travel ventrally to the pharyngeal arches and form nerves with neighboring neurons to innervate their targets (data not shown). Interestingly, a small population (35.2%) of Annexin A6-overexpressing, bipolar neurons with normal Tubb3 expression form multiple, tiny protrusions emanating from the membranes of their projections. Furthermore, those sensory neurons overexpressing Annexin A6 in the ganglionic anlage, which have yet to form bipolar processes (with Tubb3 only in their cell bodies), also possess tiny protrusions from their cell bodies. Some of these additional neuronal protrusions do not express Tubb3, implying that Annexin A6 and Tubb3 function independently of each other, with Annexin A6 controlling membrane dynamics to facilitate morphology changes required in these neurons. These gain-of-function results, together with our knockdown data, indicate that Annexin A6 itself is impacting the membrane structure of chick trigeminal sensory neurons in the absence of any effects on cytoskeletal elements such as tubulin. Our results are also in line with a prior *in vitro* study conducted on mouse lateral olfactory tract neurons, where Annexin A6 accumulates in the initial axon segment, and its overexpression significantly enhances axonal branching (Yamatani et al., 2010). Given the nature of our overexpression assay, it is remarkable that we even observed a sub-population of Annexin A6-ovexpressing neurons possessing additional processes. Annexin A6 likely interacts with other proteins in a complex that possesses a specific stoichiometry to mediate dynamic membrane changes in these neurons (discussed below), and this stoichiometry may not be achieved in all of the Annexin A6-overexpressing cells.

The Greek word “annexin” is literally defined as a “protein of bringing together,” otherwise known as a scaffolding molecule. We speculate that the role of Annexin A6 in placode cell-derived sensory neurons is, in fact, in line with this definition. Annexin A6 possesses a calcium-dependent membrane-binding domain in its C terminus (Cornely et al., 2011) (Gerke et al., 2005) that interacts with phosphotidylserine groups on the inner plasma membrane, a region rich in cholesterol and termed lipid rafts (Lizarbe et al., 2013). Previous *in vitro* studies demonstrated Annexin A6 to be a membrane scaffold that links membrane microdomains to the cytoskeleton (Cornely et al., 2011) (Saghy et al., 2015), a likely role that it is also playing in chick sensory neurons given our data. Furthermore, lipid biogenesis plays a key role in the formation of sensory nerves; for example, both rat and mouse trigeminal nerves have axonal membranes enriched in lipid rafts (Benes et al., 1973) (Gnanasekaran et al., 2011). In the chick, our results speculate on a molecular mechanism in which Annexin A6 binds to sensory neuronal membranes and acts as a scaffold to mediate the membrane changes required to generate neuronal processes (Rescher et al., 2004) (Gerke et al., 2005) (Fig. 12). In support of this, knockdown of Annexin A6, and its scaffolding function, has drastic effects on membrane biogenesis in Annexin A6-depleted sensory neurons, leading to their inability to form bipolar processes. Conversely, the membrane protrusion phenotype observed in our Annexin A6 gain-of-function studies can be ascribed

Author Manuscript Author Manuscript Author Manuscript Author Manuscript

to rearrangements of membrane microdomains or cytoskeletal elements, as suggested for other cell types overexpressing Annexin A6 (Yamatani et al., 2010).

This mechanism, in which Annexin A6 functions by changing cell membrane structure, is consistent with the role of Annexin A6 in the plasma membrane of muscle cells after injury. In this system, Annexin A6 is recruited to the membrane, leading to the formation of a "repair cap" that allows for membrane reorganization and eventual resealing, thereby healing the injury (Swaggart et al., 2014). This property of membrane repair also extends to another Annexin, Annexin A1, in epithelia and immune cells, where it orchestrates repair mechanisms during mucosal homeostasis (Leoni and Nusrat, 2016). Similarly, in mammalian myofibers upon plasma membrane injury, several Annexins (A1, A2, A5, A6) form a tight repair cap complex that is actin-dependent (Demonbreun et al., 2016). Interestingly, the repair of membranes upon muscle cell injury relies on the ordered assembly of cytosolic Annexin A6 at the membrane, creating a special scaffold to repair damaged sarcolemma (Roostalu and Strahle, 2012). Overall, our results strongly suggest that precisely regulated levels of Annexin A6 are required for the dynamic membrane restructuring events that also occur in sensory neurons during cranial gangliogenesis.

The axial position of placode cell-derived sensory neuroblasts affects the timing of their ingression and differentiation (our unpublished observations), as the chick embryo develops in an anterior-to-posterior manner. As such, pioneer neurons with bipolar processes represent "older" cells that have ingressed and migrated first, while neuroblasts that are still round or just beginning to form processes signify cells that are "younger" and have ingressed later (Moody et al., 1989). Furthermore, as sensory neurons migrate and differentiate at a specific axial level, they undergo dynamic changes in cell shape as they mature, leading to the presence of multiple cell morphologies at any given time during development (reviewed in (Breau and Schneider-Maunoury, 2015)). In support of this, we note that chick trigeminal and geniculate sensory neurons exhibit a variety of cell shapes and membrane morphologies in a static section, including round cells lacking any projections, multipolar cells with several small processes (Smith et al., 2015), and bipolar cells with two distinct processes (Fig. 12). Moreover, data from live imaging of chick trigeminal placode cell ingression and differentiation reveals dynamic membrane rearrangements in these cells (Shiau et al., 2011). Importantly, these morphological movements underscoring ingression and migration are highly conserved between chick and mouse (Nichols, 1986). Altogether, these results indicate the presence of a wide range of cell morphologies during sensory neurogenesis, at least at the axial levels examined herein for chick trigeminal and geniculate sensory neurons, in contrast to a more linear progression of cell shape changes from multipolar to bipolar as these neurons mature (Smith et al., 2015). These data further call for a reassessment of the definition of "neuronal maturation" in the context of the formation of chick trigeminal and geniculate sensory neurons, with Annexin A6 serving as one of the key molecules to mediate membrane changes necessary for the adoption of a bipolar morphology.

Author Manuscript Author Manuscript Author Manuscript Author Manuscript

CONCLUSIONS

Our data provide strong evidence for a scaffolding function for Annexin A6 within the plasma membrane of chick trigeminal and epibranchial sensory neurons. This Annexin A6-mediated scaffold is necessary to generate membrane processes, which represent morphological structures required by these sensory neurons to innervate their target tissues (Fig. 12). Sensory neurons with reduced Annexin A6 levels possess few short to no processes, while those overexpressing Annexin A6 often exhibit additional protrusions, even from the normal bipolar processes exhibited by these neurons. Interestingly, these neurons still express mature neuronal markers irrespective of the status of Annexin A6, suggesting that the membrane changes necessary to generate fully mature, sensory neurons rely upon Annexin A6 function. Collectively, these data shed additional light on molecules orchestrating sensory neurogenesis and reveal a unique role for the control of membrane dynamics by Annexin A6 during the formation of placode cell-derived neurons contributing to the cranial ganglia.

Supplementary Material

Refer to Web version on PubMed Central for supplementary material.

Acknowledgments

We thank Ms. Julia Li and Dr. Chyong-Yi Wu for their assistance with this work. The authors declare no competing financial interests. This work was supported by the National Institutes of Health (R01 DE024217 and R03 HD082421; LAT).

References

Avenali L, Narayanan P, Rouwette T, Cervellini I, Sereda M, Gomez-Varela D, Schmidt M. Annexin A2 regulates TRPA1-dependent nociception. J Neurosci. 2014; 34:14506–14516. [PubMed: 25355205]

Benes F, Higgins JA, Barrnett RJ. Ultrastructural localization of phospholipid synthesis in the rat trigeminal nerve during myelination. J Cell Biol. 1973; 57:613–629. [PubMed: 4349220]

Blentic A, Chambers D, Skinner A, Begbie J, Graham A. The formation of the cranial ganglia by placodally-derived sensory neuronal precursors. Mol Cell Neurosci. 2011; 46:452–459. [PubMed: 21112397]

Breau MA, Schneider-Maunoury S. Cranial placodes: models for exploring the multi-facets of cell adhesion in epithelial rearrangement, collective migration and neuronal movements. Dev Biol. 2015; 401:25–36. [PubMed: 25541234]

Cornely R, Rentero C, Enrich C, Grewal T, Gaus K. Annexin A6 is an organizer of membrane microdomains to regulate receptor localization and signalling. IUBMB Life. 2011; 63:1009–1017. [PubMed: 21990038]

D'Amico-Martel A, Noden DM. An autoradiographic analysis of the development of the chick trigeminal ganglion. J Embryol Exp Morphol. 1980; 55:167–182. [PubMed: 6966308]

Demonbreun AR, Quattrocelli M, Barefield DY, Allen MV, Swanson KE, McNally EM. An actin-dependent annexin complex mediates plasma membrane repair in muscle. J Cell Biol. 2016; 213:705–718. [PubMed: 27298325]

Freter S, Fleenor SJ, Freter R, Liu KJ, Begbie J. Cranial neural crest cells form corridors prefiguring sensory neuroblast migration. Development. 2013; 140:3595–3600. [PubMed: 23942515]

Gerke V, Creutz CE, Moss SE. Annexins: linking Ca2+ signalling to membrane dynamics. Nat Rev Mol Cell Biol. 2005; 6:449–461. [PubMed: 15928709]

Author Manuscript Author Manuscript Author Manuscript Author Manuscript

Gillig PM, Sanders RD. The Trigeminal (V) and Facial (VII) Cranial Nerves: Head and Face Sensation and Movement. Psychiatry (Edgmont). 2010; 7:25–31. [PubMed: 21103142]

Gnanasekaran A, Sundukova M, van den Maagdenberg AM, Fabbretti E, Nistri A. Lipid rafts control P2X3 receptor distribution and function in trigeminal sensory neurons of a transgenic migraine mouse model. Mol Pain. 2011; 7:77. [PubMed: 21958474]

Hamburger V. Experimental analysis of the dual origin of the trigeminal ganglion in the chick embryo. J Exp Zool. 1961; 148:91–123. [PubMed: 13904079]

Hamburger V, Hamilton HL. A series of normal stages in the development of the chick embryo. 1951. Dev Dyn. 1992; 195:231–272. [PubMed: 1304821]

Kerschbaum HH, Donato R, Hermann A. Annexin-immunoreactive proteins in the nervous system and eye of the gastropods, Aplysia and Helix. Brain Res. 1997; 746:133–140. [PubMed: 9037492]

Leoni G, Nusrat A. Annexin A1: shifting the balance towards resolution and repair. Biol Chem. 2016; 397:971–979. [PubMed: 27232634]

Lessner G, Schmitt O, Haas SJ, Mikkat S, Kreutzer M, Wree A, Glocker MO. Differential proteome of the striatum from hemiparkinsonian rats displays vivid structural remodeling processes. J Proteome Res. 2010; 9:4671–4687. [PubMed: 20666516]

Lizarbe MA, Barrasa JI, Olmo N, Gavilanes F, Turnay J. Annexin-phospholipid interactions. Functional implications. Int J Mol Sci. 2013; 14:2652–2683. [PubMed: 23358253]

Moody SA, Quigg MS, Frankfurter A. Development of the peripheral trigeminal system in the chick revealed by an isotype-specific anti-beta-tubulin monoclonal antibody. J Comp Neurol. 1989; 279:567–580. [PubMed: 2918088]

Naciff JM, Kaetzel MA, Behbehani MM, Dedman JR. Differential expression of annexins I–VI in the rat dorsal root ganglia and spinal cord. J Comp Neurol. 1996; 368:356–370. [PubMed: 8725344]

Nichols DH. Mesenchyme formation from the trigeminal placodes of the mouse embryo. Am J Anat. 1986; 176:19–31. [PubMed: 3487970]

Ning L, Wang C, Ding X, Zhang Y, Wang X, Yue S. Functional interaction of TRPV4 channel protein with annexin A2 in DRG. Neurol Res. 2012; 34:685–693. [PubMed: 22762361]

Park, B., Saint-Jeannet, J. Induction and Segregation of the Vertebrate Cranial Placodes. In: Kessler, DS., editor. Colloquium Series on Developmental Biology. Morgan & Claypool Life Sciences; San Rafael, CA: 2010.

Perrot R, Berges R, Bocquet A, Eyer J. Review of the multiple aspects of neurofilament functions, and their possible contribution to neurodegeneration. Mol Neurobiol. 2008; 38:27–65. [PubMed: 18649148]

Rescher U, Ruhe D, Ludwig C, Zobiack N, Gerke V. Annexin 2 is a phosphatidylinositol (4,5)-bisphosphate binding protein recruited to actin assembly sites at cellular membranes. J Cell Sci. 2004; 117:3473–3480. [PubMed: 15226372]

Rick M, Ramos Garrido SI, Herr C, Thal DR, Noegel AA, Clemen CS. Nuclear localization of Annexin A7 during murine brain development. BMC Neurosci. 2005; 6:25. [PubMed: 15819996]

Roostalu U, Strahle U. In vivo imaging of molecular interactions at damaged sarcolemma. Dev Cell. 2012; 22:515–529. [PubMed: 22421042]

Saghy E, Szoke E, Payrits M, Helyes Z, Borzsei R, Erostyak J, Janosi TZ, Setalo G Jr, Szolcsanyi J. Evidence for the role of lipid rafts and sphingomyelin in Ca2+-gating of Transient Receptor Potential channels in trigeminal sensory neurons and peripheral nerve terminals. Pharmacol Res. 2015; 100:101–116. [PubMed: 26238178]

Saint-Jeannet JP, Moody SA. Establishing the pre-placodal region and breaking it into placodes with distinct identities. Dev Biol. 2014; 389:13–27. [PubMed: 24576539]

Schiffmacher AT, Padmanabhan R, Jhingory S, Taneyhill LA. Cadherin-6B is proteolytically processed during epithelial-to-mesenchymal transitions of the cranial neural crest. Mol Biol Cell. 2014; 25:41–54. [PubMed: 24196837]

Shah A, Taneyhill LA. Differential expression pattern of Annexin A6 in chick neural crest and placode cells during cranial gangliogenesis. Gene Expr Patterns. 2015; 18:21–28. [PubMed: 25976293]

Shiau C, Lwigale P, Das R, Wilson S, Bronner-Fraser M. Robo2-Slit1 dependent cell-cell interactions mediate assembly of the trigeminal ganglion. Nat Neurosci. 2008; 11:269–276. [PubMed: 18278043]

Author Manuscript Author Manuscript Author Manuscript Author Manuscript

Shiau CE, Das RM, Storey KG. An effective assay for high cellular resolution time-lapse imaging of sensory placode formation and morphogenesis. BMC Neurosci. 2011; 12:37. [PubMed: 21554727]

Smith AC, Fleenor SJ, Begbie J. Changes in gene expression and cell shape characterise stages of epibranchial placode-derived neuron maturation in the chick. J Anat. 2015; 227:89–102. [PubMed: 26076761]

Steventon B, Mayor R, Streit A. Neural crest and placode interaction during the development of the cranial sensory system. Dev Biol. 2014; 389:28–38. [PubMed: 24491819]

Swaggart KA, Demonbreun AR, Vo AH, Swanson KE, Kim EY, Fahrenbach JP, Holley-Cuthrell J, Eskin A, Chen Z, Squire K, Heydemann A, Palmer AA, Nelson SF, McNally EM. Annexin A6 modifies muscular dystrophy by mediating sarcolemmal repair. Proc Natl Acad Sci U S A. 2014; 111:6004–6009. [PubMed: 24717843]

Wu CY, Hooper RM, Han K, Taneyhill LA. Migratory neural crest cell alphaN-catenin impacts chick trigeminal ganglia formation. Dev Biol. 2014; 392:295–307. [PubMed: 24882712]

Wu CY, Taneyhill LA. Annexin A6 modulates chick cranial neural crest cell emigration. PLoS ONE. 2012; 7:e44903. [PubMed: 22984583]

Yamanaka H, Kobayashi K, Okubo M, Noguchi K. Annexin A2 in primary afferents contributes to neuropathic pain associated with tissue type plasminogen activator. Neuroscience. 2016; 314:189–199. [PubMed: 26642807]

Yamatani H, Kawasaki T, Mita S, Inagaki N, Hirata T. Proteomics analysis of the temporal changes in axonal proteins during maturation. Dev Neurobiol. 2010; 70:523–537. [PubMed: 20225247]

Author Manuscript Author Manuscript Author Manuscript Author Manuscript

HIGHLIGHTS

- Annexin A6-depleted placodal neurons ingress, migrate, and differentiate normally.
- Mature neurons with reduced Annexin A6 do not adopt a bipolar morphology.
- Placodal neurons overexpressing Annexin A6 at times have extra membrane protrusions.
- Annexin A6 controls membrane dynamics within chick placodal neurons.

Author Manuscript Author Manuscript Author Manuscript Author Manuscript

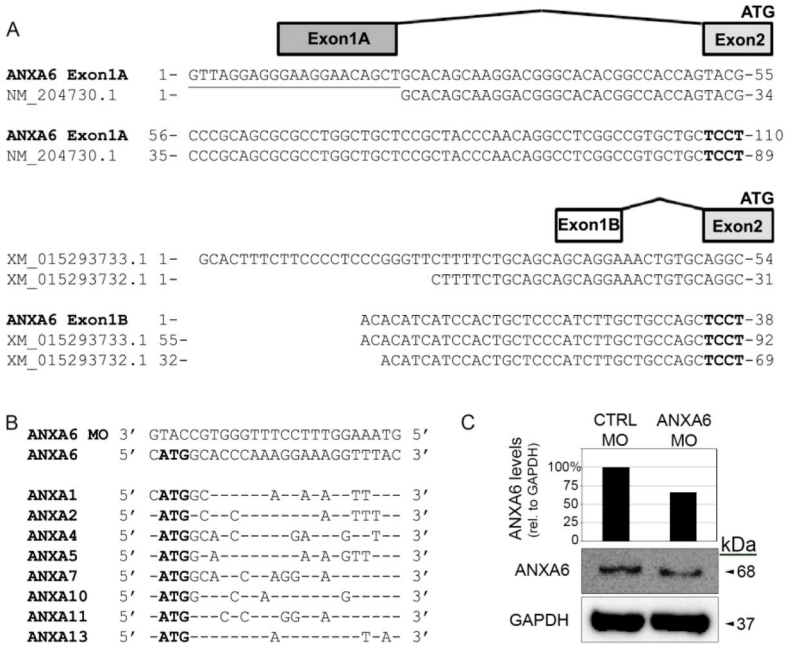

Figure 1. Two transcriptional variants of *Annexin A6* are expressed in the chick head and trigeminal ganglia and are depleted with a translation-blocking morpholino

(A) Diagram of the two transcriptional variants of *Annexin A6* identified through 5′ and 3′ RACE on RNA extracted from both HH17 heads and excised trigeminal ganglia. Transcriptional variant 1 contains a unique first exon (exon 1A) with solely 5′ UTR sequence that aligns with a confirmed NCBI sequence (accession NM_204730.1) but possesses an additional 21 nucleotides. Variant 2 contains an alternate 5′ UTR first exon (exon 1B) that aligns with two predicted NCBI variant sequences. Both variants share a conserved exon 2 splice acceptor site (exon 2 in bold), open reading frame, and 3′ UTR. (B) A translation-blocking Annexin A6 MO was designed to target the conserved start codon of both variants in (A). This MO shares 44% or less similarity with other putative *Annexin* target sites (only conserved nucleotides are shown) and also does not target other genomic sequences (not shown). (C) Knockdown efficiency of the Annexin A6 MO was assessed as previously described (Wu and Taneyhill, 2012). Immunoblot analysis reveals a 34% reduction in Annexin A6 protein as compared with the control MO-treated lysate.

Author Manuscript Author Manuscript Author Manuscript Author Manuscript

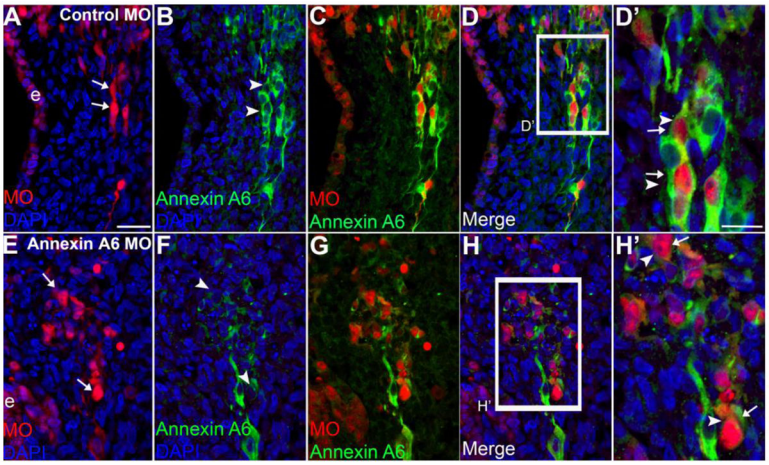

Figure 2. Morpholino-mediated depletion of Annexin A6 in trigeminal neurons has no adverse effect on their ingression, differentiation, and position within the ganglionic anlage

Representative transverse section of the forming trigeminal ganglion anlage at HH15 after electroporation of a 5 bp mismatch control Annexin A6 (A–D′) or Annexin A6 (E–H′) MO at HH10. Trigeminal placode cells electroporated with the control MO ingress normally into the ganglionic anlage (A, arrows) and maintain Annexin A6 as they differentiate into neurons (B, arrowheads). Similarly, those placode cells possessing Annexin A6 MO get correctly positioned into the ganglionic anlage (E, arrows) but lack Annexin A6 (F, arrowheads), also noted in the higher magnification merge images (D′, H′, arrows, arrowheads). DAPI (blue) labels cell nuclei. e, ectoderm. Scale bar, 50μm (A–H) and 25μm (D′, H′).

Author Manuscript Author Manuscript Author Manuscript Author Manuscript

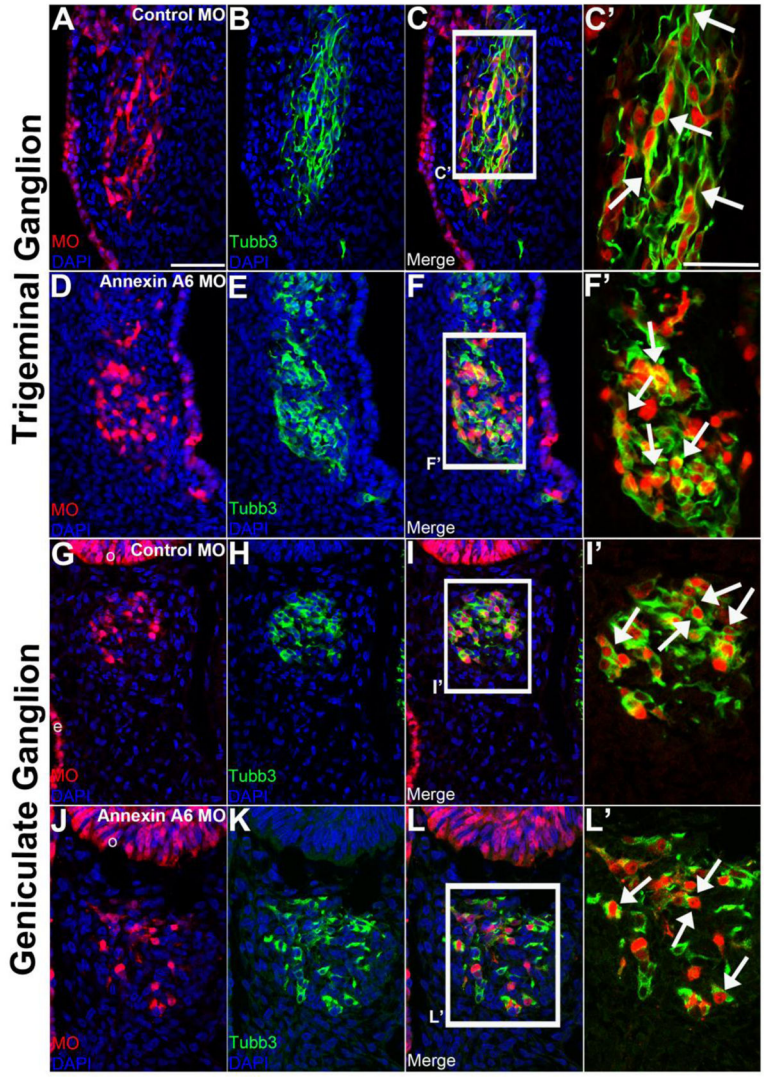

Figure 3. Annexin A6 knockdown in sensory placode cells alters the morphology of their neuronal derivatives

Representative transverse section of the forming trigeminal and geniculate ganglion at HH16 after electroporation of a 5 bp mismatch control Annexin A6 (trigeminal, A–C′; geniculate, G–I′) or Annexin A6 (trigeminal, D–F′; geniculate, J–L′) MO at HH10. Trigeminal and geniculate neurons electroporated with the control MO exhibit a bipolar morphology as seen by Tubb3 immunostaining (trigeminal, B–C′, arrows; geniculate H–I′, arrows), while those possessing Annexin A6 MO show few to no processes (trigeminal, E–F′, arrows; geniculate K–L′, arrows). DAPI (blue) labels cell nuclei. Scale bar, 50μm (A–L) and 25μm (C′, F′, I′, L′).

Author Manuscript Author Manuscript Author Manuscript Author Manuscript

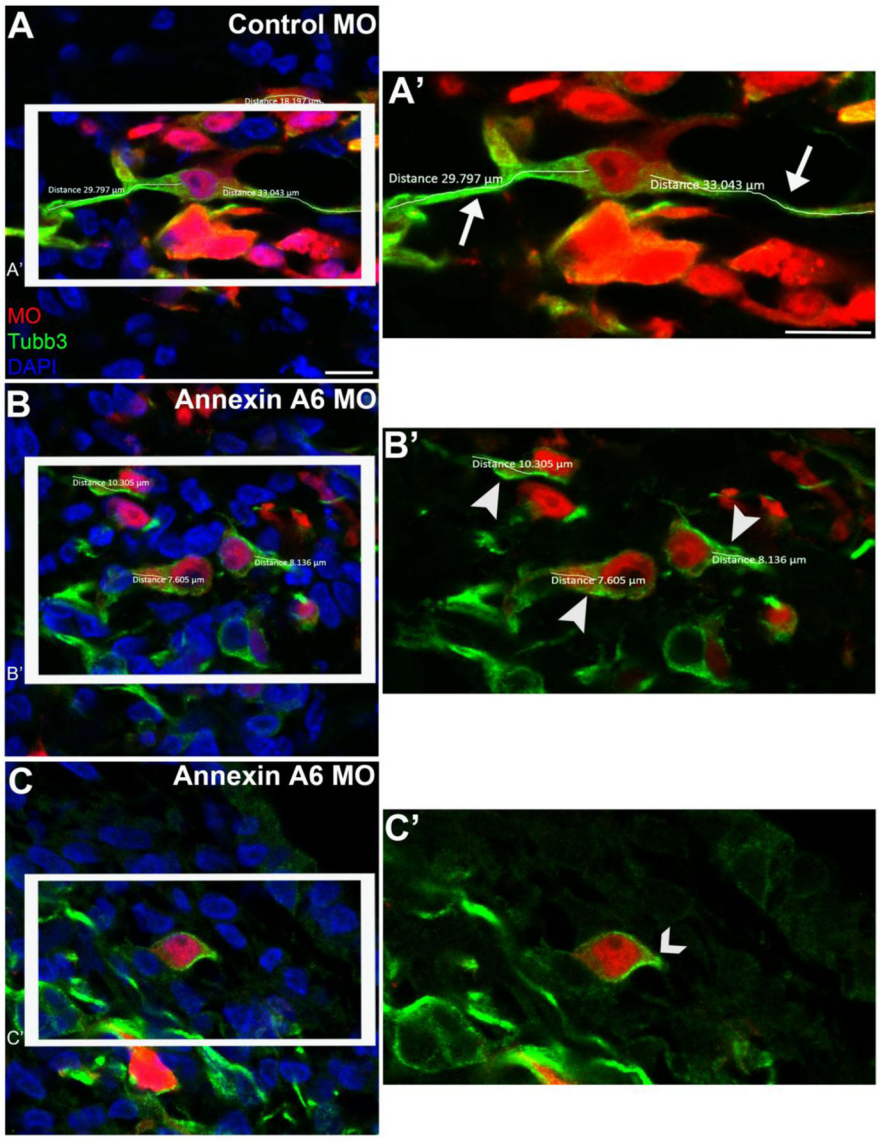

Figure 4. Annexin A6-depleted neurons possess few to no neuronal processes

Representative confocal images of trigeminal neurons containing a 5 bp mismatch control Annexin A6 (A, A') or Annexin A6 (B-C') MO at HH16. Trigeminal neurons electroporated with the control MO show bipolar projections, as seen by Tubb3 immunostaining (A), which were measured in their entirety (A', arrows), while those possessing Annexin A6 MO show few (B, B', arrowheads) to no (C, C', caret) processes. DAPI (blue) labels cell nuclei. Scale bar, 25 µm (A-C) and 12.5 µm (A', B', C').

Author Manuscript Author Manuscript Author Manuscript Author Manuscript

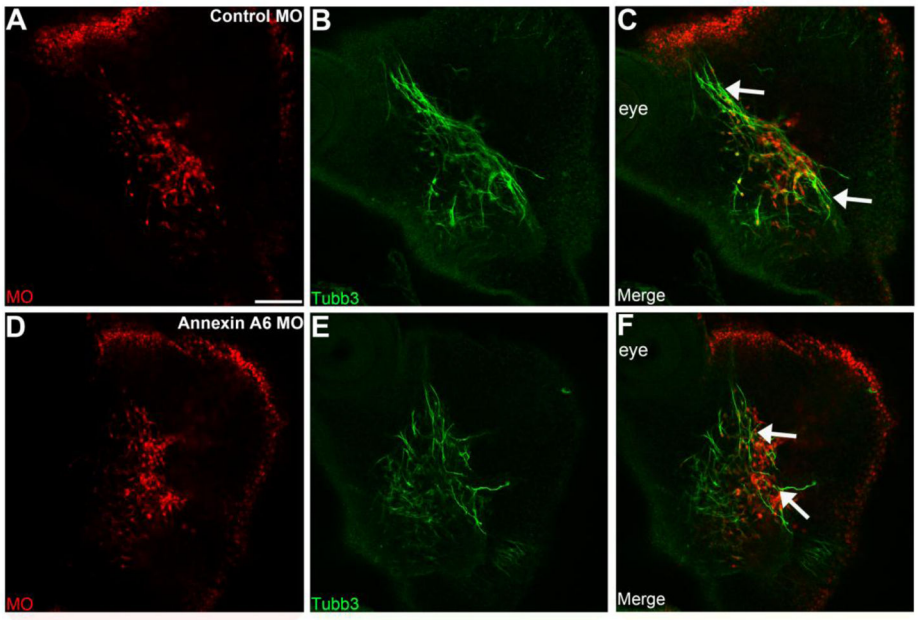

Figure 5. Annexin A6 knockdown in sensory placode cells alters the morphology of the trigeminal ganglion

Representative lateral views (optical section) of the forming trigeminal ganglion in an HH16 chick head after electroporation of a 5 bp mismatch control Annexin A6 (A-C) or Annexin A6 (D-F) MO at HH10. Trigeminal ganglia electroporated with the control MO exhibit a condensed, organized morphology, with forming nerve bundles, as seen by Tubb3 immunostaining (C, arrows), while those electroporated with the Annexin A6 MO possess a disorganized and dispersed morphology, with neurons present throughout the embryo head (F, arrows). Scale bar, 50 μm (A) applies to all images.

Author Manuscript Author Manuscript Author Manuscript Author Manuscript

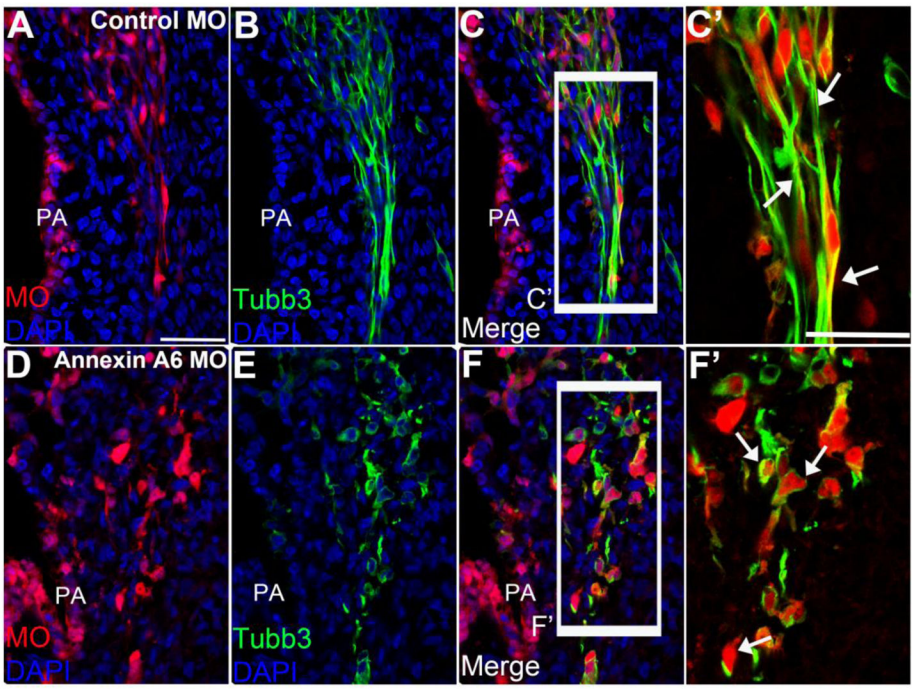

Figure 6. Annexin A6-depleted neurons lack processes to innervate their designated targets

Representative transverse section of the forming trigeminal ganglion at HH20 after electroporation of a 5 bp mismatch control Annexin A6 (A–C′) or Annexin A6 (D–F′) MO at HH10. Maxillary and mandibular branches of the trigeminal neurons electroporated with the control MO possess neuronal processes, as seen by Tubb3 immunostaining (B–C′), and form nerves with neighboring neurons to innervate the pharyngeal arch (C′, arrows). Trigeminal neurons possessing Annexin A6 MO show few to no processes (E–F′) and, consequently, do not form nerves to innervate the pharyngeal arches (F′, arrows). DAPI (blue) labels cell nuclei. PA, pharyngeal arch. Scale bar, 50μm (A–F) and 25μm (C′, F′).

Author Manuscript Author Manuscript Author Manuscript Author Manuscript

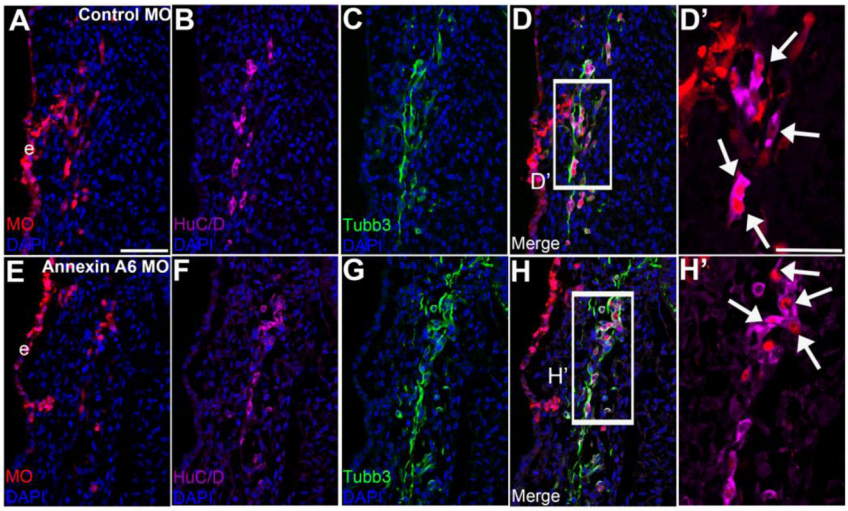

Figure 7. Trigeminal neurons with decreased Annexin A6 levels express the neuronal maturation marker HuC/D

Representative transverse section of the forming trigeminal ganglion at HH16 after electroporation of a 5 bp mismatch control Annexin A6 (A-D') or Annexin A6 (E-H') MO at HH10. Control MO-treated placode cell-derived neurons (A, D, D'), shown by Tubb3 immunoreactivity (C, D), express HuC/D (B, D, D', arrows). Annexin MO-containing cells (E, H, H') show few to no processes as noted by Tubb3 immunostaining (G, H), yet still express HuC/D (F, H, H', arrows). DAPI (blue) labels cell nuclei. e, ectoderm. Scale bar, 50 μm (A-H) and 25 μm (D', H').

Author Manuscript Author Manuscript Author Manuscript Author Manuscript

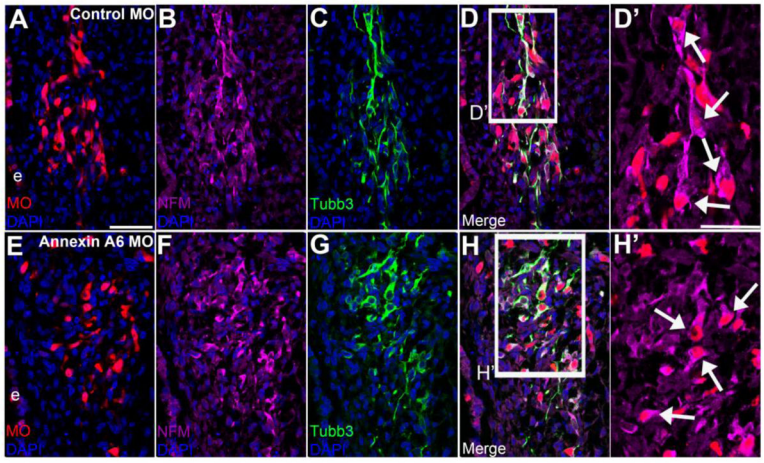

Figure 8. Annexin A6-depleted trigeminal neurons express the neuronal maturation marker NFM

Representative transverse section of the forming trigeminal ganglion at HH16 after electroporation of a 5 bp mismatch control Annexin A6 (A-D') or Annexin A6 (E-H') MO at HH10. Control MO-treated placode cell-derived neurons (A, D, D') that are Tubb3 immunoreactive (C, D) express NFM (B, D, D', arrows). Annexin MO-containing cells (E, H, H'), which possess few to no protrusions as evidenced by Tubb3 immunostaining (G, H), also express NFM (F, H, H', arrows). DAPI (blue) labels cell nuclei. e, ectoderm. Scale bar, 50 μm (A-H) and 25 μm (D', H').

Author Manuscript Author Manuscript Author Manuscript Author Manuscript

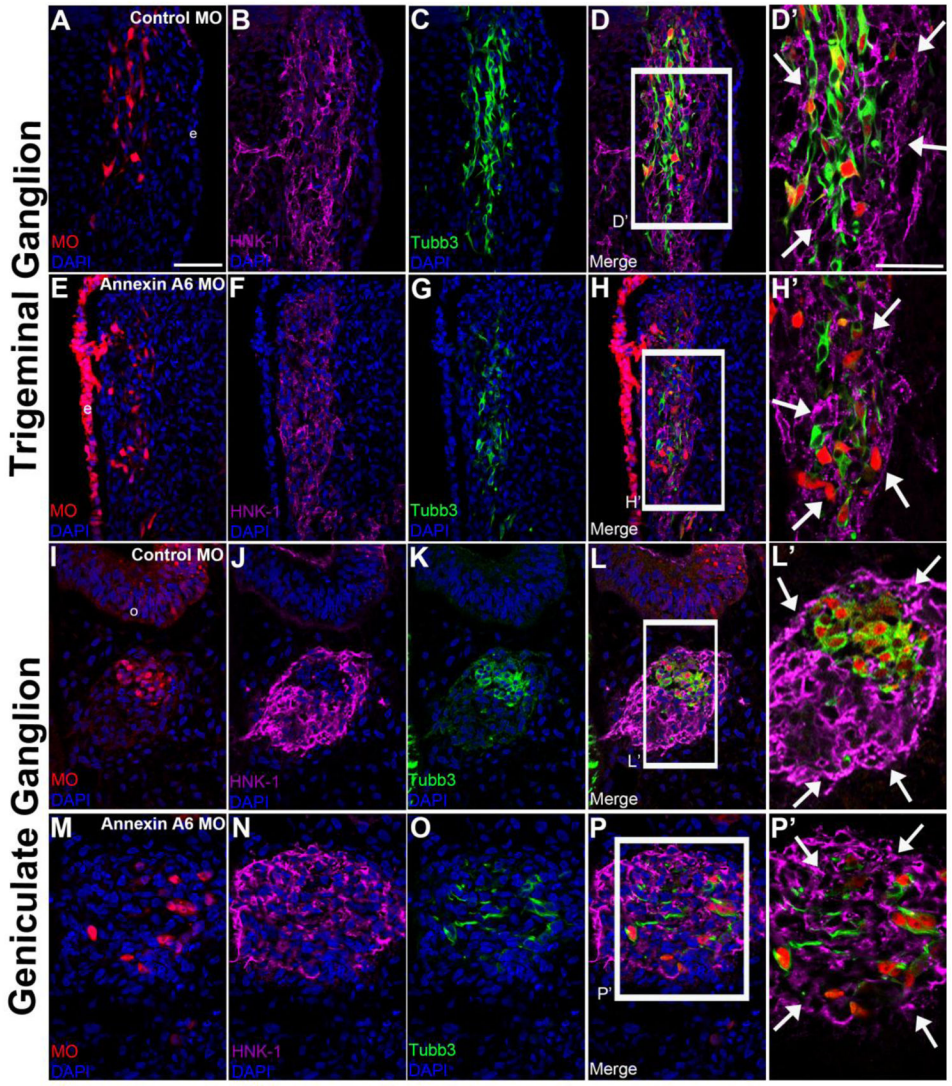

Figure 9. Neural crest cell corridors remain intact around Annexin A6-depleted sensory neurons

Representative transverse section of the forming trigeminal (A-H') and geniculate (I-P') ganglion at HH16 after electroporation of a 5 bp mismatch control Annexin A6 (A-D'; I-L') or Annexin A6 (E-H'; M-P') MO at HH10. Control MO-treated placode cell-derived neurons possess normal neural crest cell corridors (B, D, J, L; higher magnification images in D', L', arrows), as shown by HNK-1 immunostaining. This is also observed upon depletion of Annexin A6 (F, H, N, P; higher magnification images H', P', arrows). Annexin MO-containing cells possess short to no processes, as noted by Tubb3 immunostaining (G-H', O-P'). DAPI (blue) labels cell nuclei. e, ectoderm. Scale bar, 50 μm (A-P) and 25 μm (D', H', L', P').

Author Manuscript Author Manuscript Author Manuscript Author Manuscript

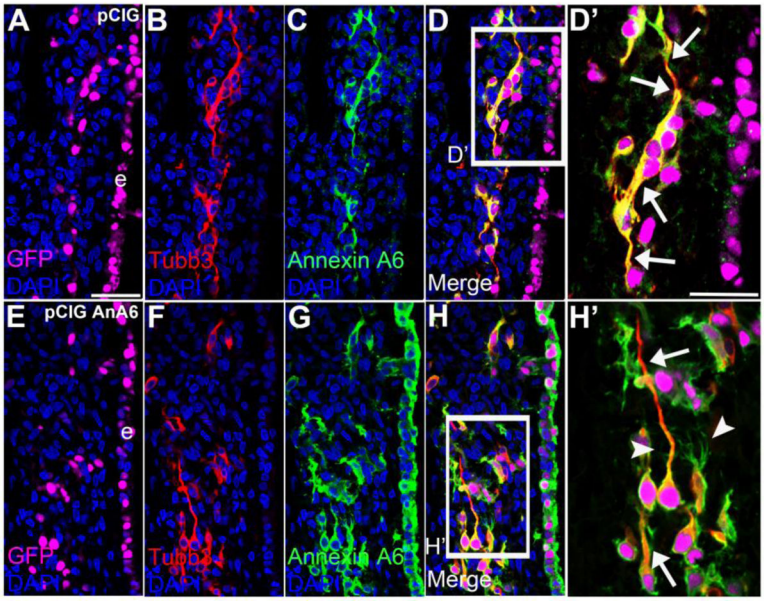

Figure 10. Annexin A6 overexpression in sensory placode cells does not affect placode cell ingression, differentiation, and position within the ganglionic anlage

Representative transverse section of the forming trigeminal and ganglion at HH16 after electroporation of pCIG control (A–D′) or pCIG-Annexin A6 (E–H′, pCIG AnA6) expression construct at HH10. Trigeminal neurons electroporated with the control pCIG (A, GFP, false-colored in purple) exhibit a bipolar morphology as seen by Tubb3 immunostaining (B, D, D′, arrows), while those overexpressing Annexin A6 (E, GFP, false-colored in purple) also show two processes through Tubb3 (F, H, H′, arrows). Some neurons containing pCIG-Annexin A6 (G–H′) possess extra protrusions emanating from their cell bodies and the membranes of their bipolar processes (H′, arrowhead). DAPI (blue) labels cell nuclei. e, ectoderm. Scale bar, 50μm (A–H) and 25μm (D′, H′).

Author Manuscript Author Manuscript Author Manuscript Author Manuscript

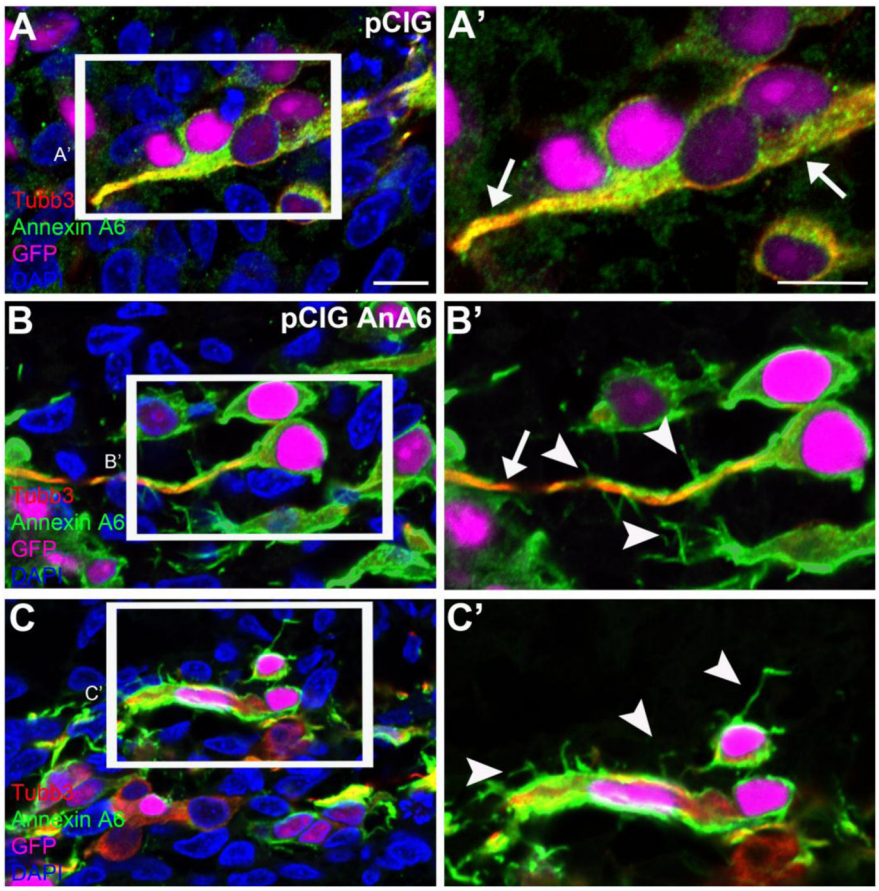

Figure 11. Annexin A6 overexpression leads to the formation of multiple tiny protrusions, in addition to bipolar processes, in some sensory neurons

Representative images of trigeminal neurons containing control pCIG (A, A′) or pCIG-Annexin A6 (B, B′, C, C′, pCIG AnA6) at HH16. Trigeminal neurons electroporated with the control pCIG vector (A, A′) show bipolar processes, as seen by Tubb3 (arrows) and Annexin A6 (arrows) immunostaining, as do those possessing pCIG-Annexin A6 (B, B′, arrow). In addition, some neurons show multiple tiny protrusions from their bipolar processes (B′, arrowheads) or cell bodies (C′, arrowheads). DAPI (blue) labels cell nuclei. Scale bar, 25μm (A–C) and 12.5μm (A′–C′).

Author Manuscript Author Manuscript Author Manuscript Author Manuscript

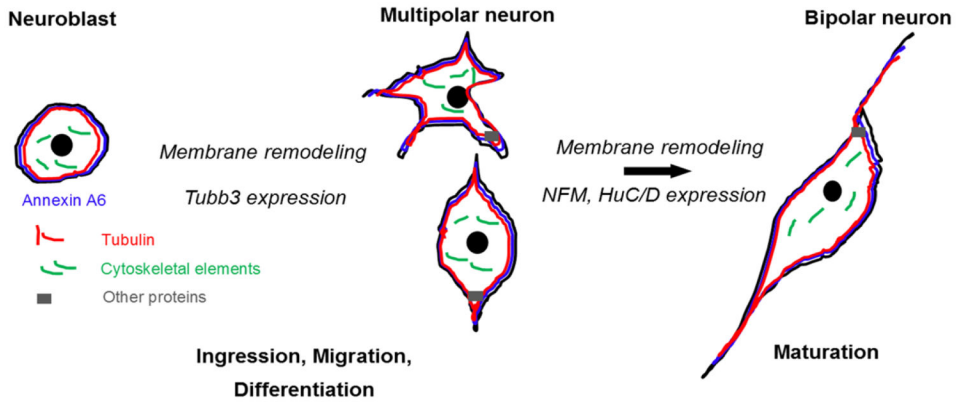

Figure 12. Annexin A6 controls the membrane dynamics, and subsequent morphology changes, accompanying the maturation of placode cell-derived neurons during chick cranial gangliogenesis

Cartoon diagram of the different morphologies adopted by sensory neurons during gangliogenesis. Sensory neuroblasts ingress from the precursor ectoderm either as cells that appear round with no processes (neuroblasts), or cells with tiny multipolar or two very short processes coming out of their cell bodies (multipolar neurons). Over the course of time, these cells mature molecularly and adopt a bipolar morphology due to the scaffolding function of Annexin A6, together with cytoskeletal rearrangements, later forming subsequent nerves.